Article

Structure and Phase State of Ti$_{49.4}$Ni$_{50.6}$ (at%) Hydrogenated in Normal Saline

Victor Grishkov, Aleksandr Lotkov [ID], Dorzhima Zhapova *, Yuri Mironov, Victor Timkin [ID], Elena Barmina and Olga Kashina

Institute of Strength Physics and Materials Science, Siberian Branch of the Russian Academy of Science, 634055 Tomsk, Russia; grish@ispms.ru (V.G.); lotkov@ispms.ru (A.L.); myp@ispms.ru (Y.M.); timk@ispms.tsc.ru (V.T.); barmina@ispms.tsc.ru (E.B.); ocash@ispms.tsc.ru (O.K.)
* Correspondence: dorzh@ispms.tsc.ru; Tel.: +7-382-228-69-82

Abstract: The paper analyzes the surface structure and phase state of Ti$_{49.4}$Ni$_{50.6}$ (at%) hydrogenated at 295 K in normal saline (0.9% NaCl aqueous solution with pH = 5.7) at 20 A/m^2 for 0.5–6 h. The analysis shows that the average hydrogen concentration in the alloy increases with the hydrogenation time t_H as follows: slowly to 50 ppm at t_H = 0.5–1.5 h, steeply to 150 ppm at t_H = 1.2–2 h, and linearly to 300 ppm at t_H = 2–6 h. According to Bragg–Brentano X-ray diffraction data (θ–2 θ, 2 θ ≤ 50°, CoKα radiation), the alloy in its scanned surface layer of thickness ~5.6 μm reveals a TiNiH$_x$ phase with x = 0.64 and x = 0.54 after hydrogenation for 4 and 6 h, respectively. The structure of this phase is identifiable as an orthorhombic hydride similar to β$_1$–TiFeH$_{0.94}$ (space group Pmcm), rather than as a tetragonal TiNiH$_x$ hydride with x = 0.30–1.0 (space group I4/mmm). Time curves are presented to trace the lattice parameters and volume change during the formation of such an orthorhombic phase from the initial cubic B2 phase in Ti$_{49.4}$Ni$_{50.6}$ (at%).

Keywords: Ti$_{49.4}$Ni$_{50.6}$ (at%) alloy; hydrogen; electrolytic hydrogenation; hydride structure

1. Introduction

TiNi alloys, showing superelasticity and shape memory, good plasticity, high corrosion resistance, and biocompatibility, are efficient materials for manufacturing various engineering devices [1,2] and medical implants [3,4]. At the same time, such alloys after their long contact with a hydrogen-containing environment, e.g., biological, are prone to embrittlement [5–8]. At near-room temperatures (290–310 K), the rate of diffusion process in TiNi is low such that a large amount of hydrogen first goes into its surface layers and then diffuses deep into the material [9,10]. As has been shown [10–12], the saturation of TiNi alloys with hydrogen decreases the temperatures of thermoelastic martensite transformations from a cubic B2 phase to a rhombohedral R and a monoclinic B19′ phase, and this impairs their superelasticity and shape memory effect [8,10,13,14] and causes their cracking and fracture [15,16]. One of the contributory factors for such functional and mechanical degradation is the formation of hydrides [16], and structural studies are needed to clarify their effect on the properties of TiNi alloys. Note that the data currently available on the state diagram of Ti-Ni-H system and the structures of hydride phases are rather scanty and contradictory.

The most comprehensive studies of such hydrides concern TiNiH$_{1.0}$ formed via saturation in gaseous hydrogen [17,18]. The studies show that this type of hydride has a tetragonal structure (space group I4/mmm) with orientation relations [100]$_H$ ∥ [100]$_{B2}$, [010]$_H$ ∥ [100]$_{B2}$, [001]$_H$ ∥ [001]$_{B2}$ and lattice parameters a_H = b_H ≈ 2 a_{B2} and c_H ≈ 4 a_{B2} [18,19]. The lattice parameters of TiNiH$_{1.0}$, according to [17,18], measure a_H = 6.221 (1) Å, c_H = 12.363 (3) Å [17] and a_H = 6.2165 (6) Å, c_H = 12.326 (1) Å [18]. From electron microscopy data [19], it follows that the hydride formed in Ti–48Ni–2Al (at%) via electrolytic hydrogenation in 4% H$_2$SO$_4$ water solution has the same tetragonal structure and space

group I4/mmm as TiNiH in TiNi after gaseous hydrogenation [17,18]. The same phase appears after electrolytic hydrogenation in NaOH water solutions: $TiNiH_x$ with x = 0.95) [20] and $TiNiH_x$ with x = 0.30 and 0.85 [21]. According to [15,21,22], electrolytic hydrogenation in both NaOH and H_2SO_4 water solutions results in a tetragonal $TiNiH_x$ phase whose lattice parameters depend on the hydrogen content. As the atomic ratio x varies from 0.30 to 0.55, the lattice parameter a_H changes from 6.09 Å to 6.25 Å and c_H from 11.40 Å to 12.60 Å. Tetragonal $TiNiH_x$ phases with x from 0.30 to 0.32 are found in Ti–50.8Ni (at%) thin wires of diameter 0.4 mm immersed in hot (90 °C) H_3PO_4 [23].

Several papers analyze the state of binary TiNi and Fe-doped TiNi after gaseous hydrogenation [24] and electrolytic hydrogenation in water solutions with 4% and 5% H_2SO_4 [25–27]. As has been found [24–26], no tetragonal hydride $TiNiH_x$ appears even at a hydrogen content in surface layers of up to 4500 ppm [24]. Instead, hydrogen-induced martensite corresponding to a monoclinic B19′ phase (space group $P2_1/m$) is formed during hydrogenation [24–27]. Such a hydrogen martensite phase appears during hydrogenation at room temperature and even in those initially B2-structured alloys which escape transformations to B19′ on cooling up to 77 K without hydrogenation. Unfortunately, no discussion of factors that may provide the absence of tetragonal $TiNiH_x$ at a high hydrogen content is presented in the cited papers [24–27].

Most of the studies of TiNi alloys hydrogenated in normal saline solutions (0.9% NaCl), e.g., [9,28–31], mainly concern the influence of hydrogenation parameters on hydrogen absorption, the effect of hydrogen on the mechanical properties of TiNi alloys (embrittlement), and the mechanisms of its thermal desorption. The structure of hydride phases is analyzed qualitatively by comparing the form of diffraction patterns after hydrogenation [28–30] with related data [17,18]. The lattice parameters of hydride phases in the majority of papers are not given. However, it is noted that certain reflections resulting from hydrogenation cannot be identified with a tetragonal hydride phase alone [9,16,23]. Besides, the presence of TiH_2 in surface layers after hydrogenation in normal saline is reported but without any confirmation [31]. Thus, the studies of hydride structures formed during hydrogenation of TiNi based alloys must be continued now.

Here we analyze the effect of electrolytic hydrogenation in normal saline (0.9% NaCl aqueous solution with pH = 5.7) on the structure and phase state of $Ti_{49.4}Ni_{50.6}$ (at%).

2. Materials and Methods

The alloy under study was $Ti_{49.4}Ni_{50.6}$ (at%) supplied as rolled plates of thickness 1.2 mm by MATEK-SMA Ltd. (Moscow, Russia). The Axiovert-200M optical microscopy (Carl Zeiss AG, Oberkochen, Germany) was used for the study of alloy microstructure. In its as-received state, the alloy had a coarse-grained structure. The shape of grains in the rolling plane was quasi-equiaxed with an average aspect ratio of 1.4, Figure 1. The average grain size in this plane was 42 μm in the rolling direction and 29 μm crosswise, and its value perpendicular to the rolling plane was 14 μm. The martensitic transformation temperatures were analyzed from temperature dependences of sample resistivity measured by four-probe potential method. The rate on cooling and heating was 3 K/min. The liquid nitrogen was used at temperatures below 300 K. The temperature dependences of sample resistivity on cooling and heating are presented in Figure 2. On cooling and heating, the alloy undergoes B2↔B19′ martensitic transformations (MT), where B2 is a CsCl-ordered cubic phase and B19′ is a monoclinic martensitic phase. The start (M_S) and finish (M_F) temperatures of B2→B19′ MT are 234 K and 163 K, respectively. The temperature range of B19′→B2 MT is from 227 K (A_S) to 252 K (A_F). Thus, at room temperature (near 295 K), the alloy had a B2 structure. It must be noted that the $Ti_{49.4}Ni_{50.6}$ (at%) alloy is used in reconstructive dentistry and cardiovascular implantation like the binary TiNi based alloys with 50.7 and 50.8 at% Ni.
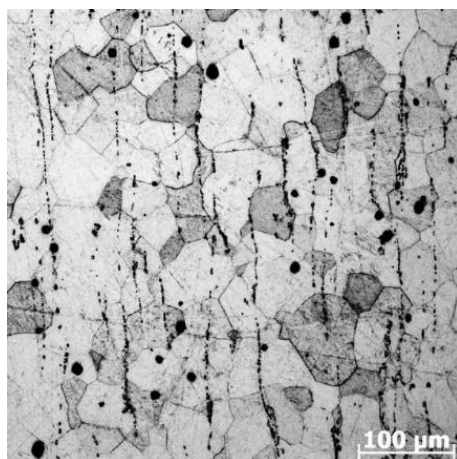
Figure 1. The optical microscopy image of microstructure in $Ti_{49.4}Ni_{50.6}$ (at%) samples in rolling plane.
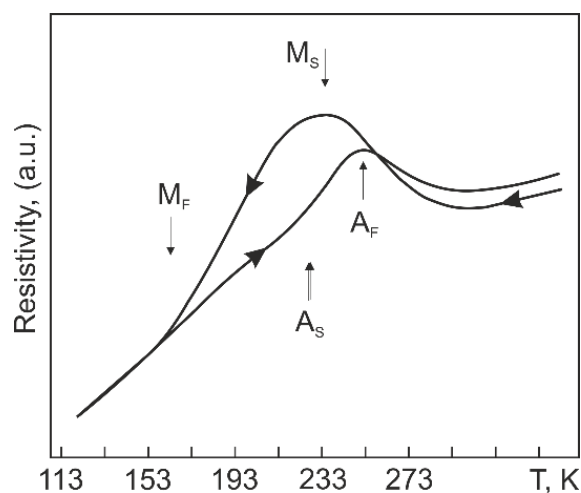

Figure 2. Temperature dependences of electrical resistivity on cooling and heating of initial samples.

For studying the hydrogen distribution and phase state of $Ti_{49.4}Ni_{50.6}$ (at%), the specimens were shaped as plates of dimensions 10 mm × 10 mm and thickness 1.13 mm. Its specimens for studying the average hydrogen concentration were square bars of cross-section 1.1 mm × 1.1 mm and length 50 mm. Both the plates and the bars were mechanically grinded using an abrasive paper with gradual decrease in its grit to 2000 (Automotive Aftermarket 3M United Kingdom PLC, Market Place Bracknell, Berks, UK), polished with a diamond paste grained to 0.6 μm (Pasta Diamanta, Corsico (MI), Italy) and rinsed in ethanol and warm distilled water.

The specimens were hydrogenated at room temperature (295 K) in normal saline (0.9% NaCl aqueous solution with pH = 5.7) at a current density of 20 A/m² for 0.5–6 h. The increase of electrolyte temperature was about 2 K after hydrogenation for 6 h.

The structure and the phase state of $Ti_{49.4}Ni_{50.6}$ (at%) were analyzed at 295 K on a DRON-7 diffractometer (CoK_α radiation) with PDWin software (JSC IC Burevestnik, St. Petersburg, Russia). It should be noted that in this geometry, the thickness of layers with 95% of the diffraction intensity in CoK_α radiation is 2.3–2.9 μm at 2 θ = 20°–25° and 3.5–5.6 μm at 2 θ = 40°–50°, according to estimations proposed elsewhere [32]. The average hydrogen content in $Ti_{49.4}Ni_{50.6}$ (at%) was determined on a LECO RHEN 602 gas analyzer (Saint Joseph, MI, USA). The hydrogen distribution in $Ti_{49.4}Ni_{50.6}$ (at%) was studied by glow-discharge optical emission spectrometry on a GD OES Profiler 2 (Jobin Yvon Emission Horiba Group, Longjumeau Cedex, France). This method is based on the sputtering of

the material of the samples, which are the cathode in the plasma of a glow discharge in argon. The atomized atoms of the sample material are excited and ionized in the glow discharge plasma and emit characteristic radiation. This radiation is analyzed with an optical spectrometer. The sputtering of the sample with argon ions is continuously, layer by layer, as the depth of the erosion crater increases. This makes it possible to obtain profiles of the distribution of elements in the surface layers of the samples by registering the signal of the optical spectrometer depending on the sputtering time. The quality of the analysis depends on the shape of the craters. The craters formed during the sputtering of the $Ti_{49.4}Ni_{50.6}$ (at%) samples had vertical walls and a flat bottom, which is optimal. The depth of craters after sputtering for 900 s was 50 ± 3 µm. The average content of hydrogen and its distribution profiles in $Ti_{49.4}Ni_{50.6}$ (at%) was determined within 1 h after hydrogenation.

3. Results

Figure 3 shows the average hydrogen concentration C_H in $Ti_{49.4}Ni_{50.6}$ (at%) versus the hydrogenation time t_H. It is seen that at up to $t_H = 1$ h, the absorption of hydrogen is slight. The average hydrogen concentration measures 50 wt. ppm (or ppm) even at $t_H = 1.5$ h. After hydrogenation for 1.5 h, its value increases steeply, reaching $C_H = 150$ ppm at $t_H = 2$ h. As the hydrogenation time is increased from 2 to 6 h, the average hydrogen concentration increases almost linearly to $C_H = 300$ ppm. The behavior of C_H in Figure 3 characterizes $Ti_{49.4}Ni_{50.6}$ (at%) with a uniform hydrogen distribution in its volume. However, directly after hydrogenation, the hydrogen distribution over the alloy cross-section is rather nonuniform. Figure 4 shows the cross-sectional hydrogen distribution versus the hydrogenation time t_H. The profiles in Figure 4 qualitatively characterize the hydrogen distribution because the ordinate is not the absolute concentration of hydrogen but the signal amplitude proportional to its concentration (in the first approximation). The lower abscissa axis is the sputtering time, and the upper one is the depth from the alloy surface calculated for respective time points on the assumption of equal sputtering rates of the hydrogenated layer and initial material far from it.
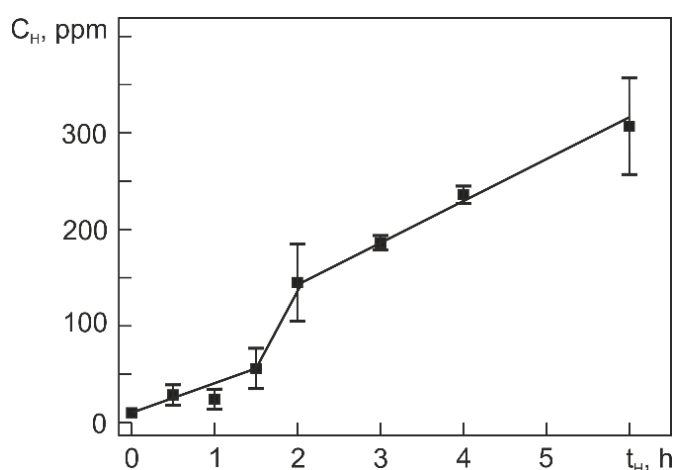

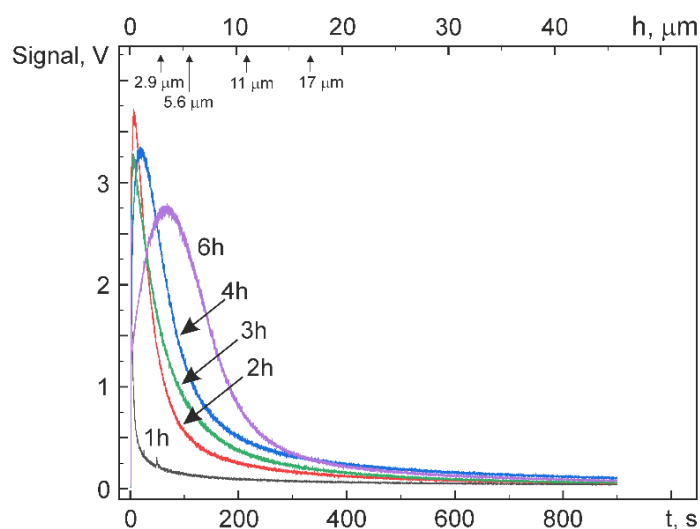**Figure 3.** Hydrogen concentration vs. hydrogenation time in $Ti_{49.4}Ni_{50.6}$ (at%).

Figure 4. Qualitative profiles of signal distribution due to hydrogen atoms vs. sputtering time in $Ti_{49.4}Ni_{50.6}$ (at%) after electrolytic hydrogenation in normal saline. (This figure is in color only in the electronic version.)

It is seen from Figure 4 that the localization of hydrogen peaks in $Ti_{49.4}Ni_{50.6}$ (at%) falls on its near surface region (3–4 μm thick) and that the highest peak occurs after hydrogenation for 2 h. As t_H is increased to 6 h, the signal gets smaller. By and large, the thickness of the layer with high hydrogen content increases monotonically with t_H due to hydrogen diffusion deep into the material. Figure 5 shows the depth $L_{0.1}$ at which the signal level measures 10% of its near-surface maximum, allowing us to qualitatively judge the layer thickness with a high hydrogen content compared to its value in the initial alloy (10 ppm). It is seen from Figure 5 that the layer rich in hydrogen almost linearly increases in thickness to ~17 μm as t_H is increased to 6 h. Thus, about 90% of hydrogen atoms are concentrated in zones of thickness 11 μm and 17 μm after hydrogenation for 4 and 6 h, respectively. Note that the thickness of these zones is close to the average grain size in a direction normal to the rolling plane (14 μm) coincident with the surface samples. The maximum hydrogen content is in a narrow surface zone (Figure 4) whose width is smaller than $L_{0.1}$ (Figure 5).
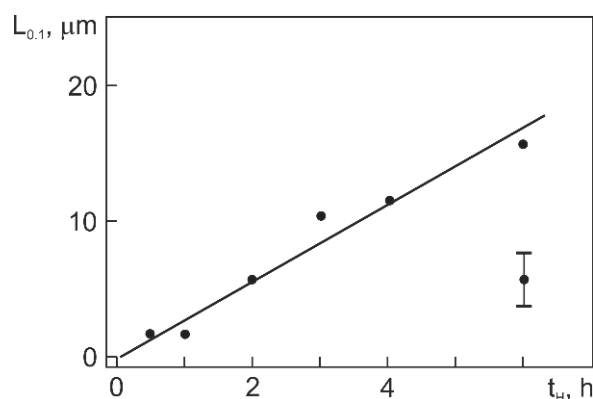
Figure 5. Depth $L_{0.1}$ with hydrogen signal level of 10% from its maximum vs. hydrogenation time in $Ti_{49.4}Ni_{50.6}$ (at%).

The surface structure and phase state of $Ti_{49.4}Ni_{50.6}$ (at%) after hydrogenation at 295 K for different times can be judged from Figure 6, showing its diffraction patterns in the Bragg–Brentano geometry (θ–2 θ, CoK_α radiation). As it was noted above, the thickness of analyzed layers equals 2.3–2.9 μm at 2 θ = 20°–25° and 3.5–5.6 μm at 2 θ = 40°–50°.

Thus, the diffraction patterns in Figure 6 reflect the evolution of the structure and phase state of hydrogenated layers whose thickness is close to the surface layer thickness with a maximum hydrogen content and is no greater than ~40% of the average grain size in this direction. It is seen from Figure 6 that before hydrogenation, only a $(110)_{B2}$ peak at $2\theta \approx 49.7°$ is detected in the range of diffraction angles $2\theta \leq 50°$. However, even after hydrogenation for 0.5 h, the alloy reveals a weak peak at $2\theta \approx 22°$, and after hydrogenation for 1 and 1.5 h, two peaks at $2\theta \approx 22°$ and $2\theta \approx 45°$, respectively, and an increase in the $(110)_{B2}$ asymmetry. After hydrogenation for 3 h and longer, a peak at $2\theta \approx 48°$ appears. Increasing the hydrogenation time to $t_H = 6$ h shifts the $(110)_{B2}$ peak from $2\theta \approx 49.7°$ to the range of smaller diffraction angles, suggesting that the corresponding interplanar spacing gets larger. The peak intensity at about $2\theta = 22°$ and $45°$ increases most rapidly with increasing t_H to 1.5–2 h, and further, this increase slows down (Figure 7).
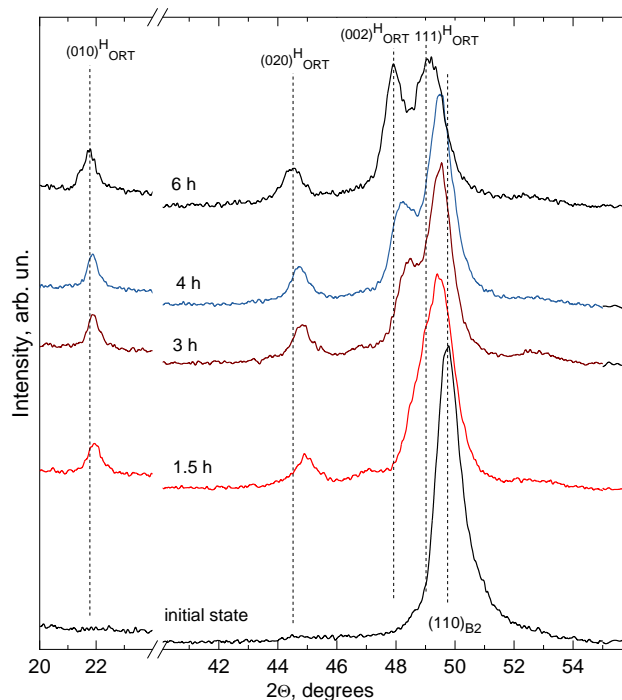
Figure 6. X-ray diffraction patterns of $Ti_{49.4}Ni_{50.6}$ (at%) before and after hydrogenation at 295 K in normal saline for 1.5, 3, 4, and 6 h (20 A/m^2). (This figure is in color only in the electronic version.)

Figure 7. Peak intensity at $2\Theta \approx 22°$ (o) and $2\Theta \approx 45°$ (●) vs. hydrogenation time.

Such peak intensities correlate with hydrogen distributions in a surface zone ~5.6 μm thick: after hydrogenation for more than 2 h, hydrogen starts actively diffusing from this

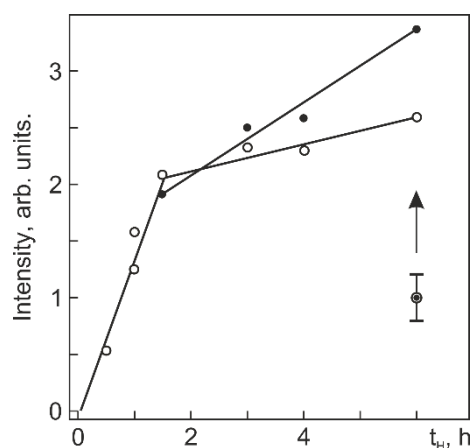zone deep into the alloy but its concentration through a thickness of 2.9–5.6 μm becomes maximal after hydrogenation for 6 h (Figure 4). Thus, the absorption of hydrogen by $Ti_{49.4}Ni_{50.6}$ (at%) during electrolytic hydrogenation leads to the formation of the hydride phase in its surface zone measuring no less than 5.6 μm. The structure of this phase is analyzed in detail below.

4. Discussion

Of importance for our further analysis is to estimate the hydrogen content in the surface layers of hydrogenated samples (zones with thickness ≤ 5.6 μm). This estimation is based on the average hydrogen concentration C_H (Figure 4) and the thickness of layers $L_{0.1}$ in which the content of absorbed hydrogen is high (Figure 5). Let us assume that the total content of hydrogen with its average concentration C_H (Figure 5) is uniformly distributed in a layer of thickness $L_{0.1}$. Then, the average hydrogen concentration in this layer can be estimated as follows:

$$C_H(L_{0.1}) = \frac{C_H}{4\left[\left(\frac{L_{0.1}}{T}\right) - \left(\frac{L_{0.1}}{T}\right)^2\right]}, \tag{1}$$

where T is the specimen thickness (1.13 mm). In the specimens hydrogenated for 4 and 6 h, C_H equal, respectively, to 230 ppm and 300 ppm (1.20 at% and 1.56 at%) and $L_{0.1}$ equal to 11 μm and 17 μm. Then, $C_H(L_{0.1})$ equal, respectively, ~6000 ppm and ~ 5000 ppm in these specimens. However, the actual hydrogen distribution is nonuniform: the hydrogen content is highest near the surface and decreases in going deep from the surface to $L_{0.1}$. Assuming (in the first approximation) that the hydrogen content decreases linearly through $L_{0.1}$, its maximum near the surface will be about twice higher than $C_H(L_{0.1})$, i.e., ~12,000 ppm and ~10,000 ppm after hydrogenation for 4 and 6 h, respectively. It is easy to show that the maximum hydrogen content in the surface layer of $Ti_{49.4}Ni_{50.6}$ (at%) hydrogenated for 4 and 6 h is ~39.0 at% and ~35.1 at% and that the approximate chemical composition of the layer in the two cases is represented by $Ti_{30.1}Ni_{30.9}H_{39.0}$ and $Ti_{32.0}Ni_{32.9}H_{35.1}$ (at%), respectively.

The hydrogen content can be estimated in weight units (ppm) and atomic percent, and also as the ratio of absorbed hydrogen atoms to metal atoms:

$$x = \frac{N_H}{N_{Me}} = \frac{N_H}{N_{Ti} + N_{Ni}} = \frac{a_H}{100 - a_H}, \tag{2}$$

where Me is the number of Ti and Ni atoms and a_H is the hydrogen content in atomic percent. Then, the chemical composition of surface zones is represented by $TiNiH_{0.64}$ and $TiNiH_{0.54}$ after hydrogenation for 4 and 6 h, respectively.

It should be noted that the diffraction patterns obtained in our study differ greatly from those typical of TiNi alloys with a monoclinic B19' and a hydrogen martensite structure (in particular, in interplanar spacing). The identification of $TiNiH_x$ on the assumption of its tetragonal structure (with x = 0.30–0.55 [15,22] or x =1 [17–19]) is also doubtful because a rather large discrepancy is found between the lattice parameters of tetragonal $TiNiH_{0.54}$ after hydrogenation for 6 h and those of $TiNiH_{0.55}$ [15,22]: *a* = 6.00 Å, *c* = 11.26 Å against *a* = 6.25 Å, *c* = 12.60 Å, respectively. Besides, the volume changes induced by these hydrides of approximate composition differ even in sign: $(V_H–16V_{B2})/16V_{B2}$ = + 11.7% for $TiNiH_{0.55}$ [15,22] and –4.4% for $TiNiH_{0.54}$ (after hydrogenation in saline for 6 h). Hence, the available data give no way of reliably identifying the hydride structure formed in $Ti_{49.4}Ni_{50.6}$ (at%) during electrolytic hydrogenation in normal saline (0.9% NaCl). In this connection, let us extend our analysis to $TiMeH_x$ in B2-structured TiMe alloys. According to [33], the hydrides formed in TiFe during saturation in gaseous hydrogen are orthorhombic $TiFeH_{0.94}$ and $TiFeH_{1.40}$ (space group D_{2h}^5 – Pmcm) with lattice parameters *a* = 2.954 (1) Å, *b* = 4.538 (1) Å, *c* = 4.381 (1) Å and *a* = 3.094 (3) Å, *b* = 4.513 (4) Å, *c* = 4.391 (10) Å, respectively. The most intense reflections of these hydrides are due to their orthorhombic structure: (111), (002), (020), and (010) in order of increasing interplanar

spacing. Between the reflections (010) and (020), only (011), (100), and (110) are resolved but their intensity measures 1–2% of the 100% intensity of the strongest reflection (111). The probability of identifying these reflections on X-ray diffraction patterns is low, particularly in view of the coarse-grained structure and texture of rolled specimens. In general, the diffraction patterns of $TiFeH_{0.94}$ and $TiFeH_{1.40}$ presented in the cited paper [33] are qualitatively the same as those suggesting the presence of an orthorhombic hydride phase in Figure 6 with its lattice parameters versus the hydrogenation time in Figure 8.
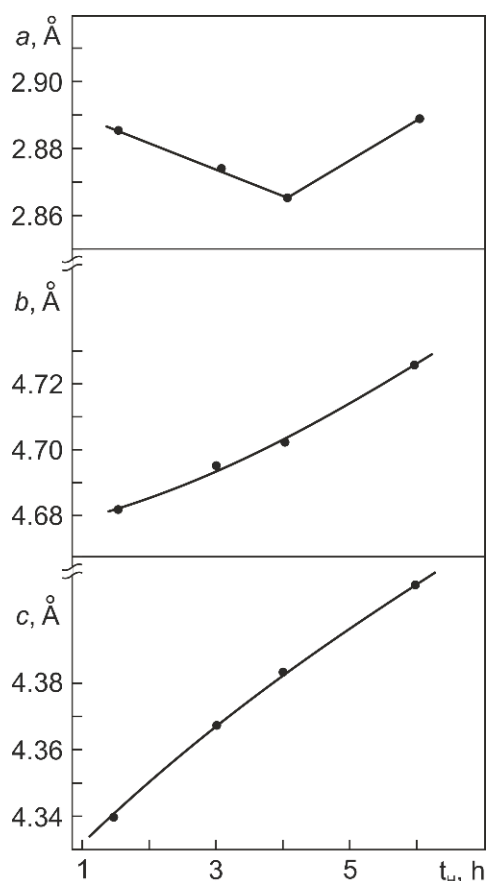

Figure 8. Lattice parameters(a, b and c) of orthorhombic hydride (analogue of β_1-$TiFeH_{0.94}$) vs. hydrogenation time t_H in normal saline at 20 A/m^2.

It is seen in Figure 8 that as the hydrogenation time (and, hence, the amount of absorbed hydrogen) is increased, the lattice parameter *a* first decreases (t_H = 1.5–4 h) and then increases (t_H > 4 h) while the parameters *b* and *c* grow monotonically with t_H. The absolute values of the lattice parameters in Figure 8 suggest that the orthorhombic structure of $TiNiH_{0.54}$, like the tetragonal structure of $TiNiH_x$ with x = 0.30–0.55, has orientation relations with the initial B2 structure. Behind this assumption is the following reasoning. In Cu-doped TiNi alloys (in particular, in $Ti_{49.5}Ni_{49.5}Cu_{10}$ (at%) [34]), a B19 martensite phase with a similar orthorhombic structure (space group D_{2h}^5 – Pmmb) and lattice parameters a = 2.881 Å, b = 4.279 Å, c = 4.514 Å is formed via B2→B19 transformation. The B19 phase has the following orientation relations with the initial B2 phase: $[100]_{B19} \parallel [100]_{B2}$, $[010]_{B19} \parallel [01\bar{1}]_{B2}$, $[001]_{B19} \parallel [011]_{B2}$ [34]. During its formation, $a_{B19} < a_{B2}$ (3.030 Å), $b_{B19} \approx a_{B2}\sqrt{2}$ (4.285 Å), and $c_{B19} > a_{B2}\sqrt{2}$. On the assumption of similar orientation relations for orthorhombic $TiNiH_{0.54}$, whose lattice parameters are presented in Figure 8, we can estimate the volume change induced by the formation of this phase. From Figure 9, it is seen that as the hydrogenation time is increased from 1.5 to 6 h, the ratio $\Delta V/2V_{B2} = (V_H - 2V_{B2})/2V_{B2}$ increases almost linearly from +7.3% to +10.2%. Note that the volume changes induced

by the formation of orthorhombic $TiNiH_{0.54}$ (after hydrogenation for 6 h) and tetragonal $TiNiH_{0.55}$ [15,22] are positive and close: +10.2% and +11.3% [15,22], respectively.
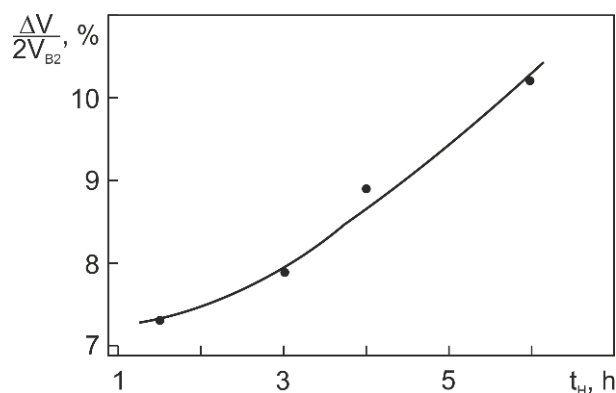

Figure 9. Volume change induced by orthorhombic hydride vs. hydrogenation time.

Surely, such an orthorhombic hydride structure needs a more detailed confirmation (including its confirmation by transmission electron microscopy). At the same time, our research data suggest that not only a tetragonal hydride, but other hydride structures may arise in TiNi alloys during hydrogenation.

5. Conclusions

1. Our study of $Ti_{49.4}Ni_{50.6}$ (at%) hydrogenated at 295 K in normal saline at 20 A/m^2 for 0.5–6 h shows that the average concentration of absorbed hydrogen increases with the hydrogenation time t_H as follows: slowly to 50 ppm at t_H = 0.5–1.5 h, steeply to 150 ppm at t_H = 1.5–2 h, and linearly to 300 ppm at t_H = 2–6 h. Increasing the hydrogenation time increases the diffusion of hydrogen deep into the alloy. The hydrogen-rich layer thickness increases linearly with t_H, measuring ~17 μm at t_H = 6 h.
2. The maximum content of absorbed hydrogen in the alloy falls within its surface layer ~5.6 μm thick, which is equal to the layer scanned for diffraction with CoK_α radiation in the θ–2θ geometry at 2θ ≤ 50°. The composition of this layer corresponds to $TiNiH_x$ with x = 0.64 and x = 0.54 (atomic ratio of hydrogen to Ti plus Ni) after hydrogenation for 4 and 6 h, respectively.
3. It is shown that no hydride phase reflections are identified, assuming the presence of the known hydride phase $TiNiH_x$ (x from 0.30 to 1.0) with tetragonal structure (space group I4/mmm).
4. It was found that the structure of hydride phase formed in $Ti_{49.4}Ni_{50.6}$ (at%) during hydrogenation is similar to the structure of orthorhombic $β_1$-$TiFeH_{0.94}$ hydride phase (space group Pmcm). After hydrogenation for 6h, the lattice parameters of $TiNiH_{0.54}$ orthorhombic hydride phase are a_H = 2.890 Å, b_H = 4.726 Å, c_H = 4.410 Å and the volume change induced by it is +10.2%.

Author Contributions: Conceptualization, A.L. and V.G.; methodology, A.L. and V.G.; software V.T. and Y.M.; validation, A.L., V.G. and D.Z.; formal analysis, A.L., V.G., D.Z. and Y.M.; investigation, V.G., D.Z., Y.M., V.T., E.B. and O.K.; writing—original draft preparation, V.G.; writing—review and editing, V.G., A.L. and D.Z.; supervision, A.L., V.G., V.T. and D.Z.; project administration, A.L., V.G. and D.Z.; funding acquisition, A.L. and D.Z. All authors have read and agreed to the published version of the manuscript.

Institutional Review Board Statement: Not applicable.

Informed Consent Statement: Not applicable.

Conflicts of Interest: The authors declare no conflict of interest.

References

1.   Duerig, T.W.; Melton, K.N.; Stöckel, D.; Wayman, C.M. *Engineering Aspects of Shape Memory Alloys*, 1st ed.; Butterworth-Heinemann: Oxford, UK, 1990; p. 499.

2.   Tikhonov, A.S.; Gerasimov, A.P.; Prokhorova, I.I. *Shape Memory Effects in Modern Engineering*; Mashinostroenie: Moscow, Russia, 1981; p. 81. (In Russian)

3.   Zhuravlev, V.N.; Pushin, V.G. *Alloys with Thermomechanical Memory and Their Application in Medicine*; UrB RAS: Ekaterinburg, Russia, 2000; p. 150. (In Russian)

4.   Kapoor, D. Nitinol for Medical Applications: A Brief Introduction to the Properties and Processing of Nickel Titanium Shape Memory Alloys and their Use in Stents. *Johns. Matthey Technol. Rev.* **2017**, *61*, 66–67. [CrossRef]

5.   Harris, E.F.; Newman, S.M.; Nicholson, J.A. Nitinol arch wire in a simulated oral environment: Changes in mechanical properties. *Am. J. Orthod. Dentofac. Orthop.* **1988**, *93*, 508–513. [CrossRef]

6.   Montero-Osampo, C.; Lopez, H.; Salinas Rodriguez, A. Effect of compressive straining on corrosion resistance of a shape memory Ni-Ti alloy in Ringer's solution. *J. Biomed. Mater. Res.* **1996**, *32*, 583–591. [CrossRef]

7.   Yokoyama, K.; Hamada, K.; Moriyama, K.; Asaoka, K. Degradation and fracture of Ni-Ti superelastic wire in an oral cavity. *Biomaterials* **2001**, *22*, 2257–2262. [CrossRef]

8.   Asaoka, K.; Yokoyama, K.; Nagumo, M. Hydrogen embrittlement of nickel-titanium alloy in biological environment. *Metallurg. Mater. Trans. A* **2002**, *33*, 495–501. [CrossRef]

9.   Yokoyama, K.; Ogawa, T.; Takashima, K.; Asaoka, K.; Sakai, J. Hydrogen embrittlement of Ni-Ti superelastic alloy aged at room temperature after hydrogen charging. *Mat. Sci. Eng. A* **2007**, *466*, 106–113. [CrossRef]

10. Baturin, A.; Lotkov, A.; Grishkov, V.; Rodionov, I.; Zhapova, D. Effect of Hydrogen Redistribution during Aging on the Martensitic transformation and Superelasticitiy of Nanocrystalline TiNi Alloy. *J. Metastab. Nanocryst. Mater.* **2019**, *31*, 30–34. [CrossRef]

11. Runciman, A.; Chen, K.C.; Pelton, A.R.; Trépanier, C. Effects of Hydrogen on the Phases and Transition Temperatures of NiTi. In Proceedings of the International Conference on Shape Memory and Superelastic Technologies, Asilomar Conference Center, Pacific Grove, CA, USA, 7–11 May 2006; Berg, B., Mitchell, M.R., Proft, J., Eds.; ASM International: Materials Park, OH, USA, 2006; pp. 185–196, ISBN 0871708620/9780871708625.

12. Baturin, A.; Lotkov, A.; Grishkov, V.; Rodionov, I.; Bordulev, Y.; Kabylkakov, Y. Hydrogen diffusion and the effect oh hydrogen on structural transformations in binary TiNi based alloys. *Int. J. Hydrog. Energy* **2019**, *44*, 29371–29379. [CrossRef]

13. Adachi, Y.; Wade, N.; Hosoi, Y. Effect of Hydrogen on the Shape Memory Effect and Transformation Behavior of Ti-Ni Alloys. *J. Japan Inst. Metals* **1990**, *54*, 525–531. [CrossRef]

14. Asaoka, T. Superelastic Properties of Ti-Ni-Cu Alloy Under Mild Hydrogen Absorbing Condition. *J. Phys. IV* **1995**, *5*, 723–728. [CrossRef]

15. Hagi, H.; Mizuno, M.; Ibe, T. Hydrogen Embrittlement of 50.9at%Ni-Ti Alloy Caused by Cathodic Polarization. *J. Surf. Finish. Soc. Jap.* **1997**, *48*, 826–831. [CrossRef]

16. He, J.Y.; Gao, K.W.; Su, Y.J.; Qiao, L.J.; Chu, W.Y. The effect of hydride and martensite on the fracture toughness of TiNi shape memory alloy. *Smart Mater. Struct.* **2004**, *13*, N24–N28. [CrossRef]

17. Noreus, D.; Werner, P.-E.; Alasafi, K.; Schmidt-Ihn, E. Structural studies of TiNiH. *Int. J. Hydrog. Energy* **1985**, *10*, 547–550. [CrossRef]

18. Soubeyroux, J.L.; Fruchart, D.; Lorthioir, G.; Ochin, P.; Colin, D. Structural Study of Hydrides $NiTiH_x$ (x = 1.0 and 1.4). *J. Alloys Comp.* **1993**, *196*, 127–132. [CrossRef]

19. Nam, T.H.; Shimizu, K.; Saburi, T.; Nenno, S. Crystal Structure of a Hydride Formed by Electrochemical Hydrogenation n a Ti-Ni-Al Alloys. *Mater. Trans. JIM* **1989**, *30*, 539–548. [CrossRef]

20. Fruchart, D.; Soubeyroux, J.L.; Miragllia, S.; Obbade, S.; Lorthioir, G.; Basile, F.; Colin, C.; Faudot, F.; Ochin, P.; Dezellus, A. Structural Transformations in NiTi, a Potensial Materials for Hydrogen Storage. *Z. Phys. Chem.* **1993**, *179*, 225–236. [CrossRef]

21. Basile, F. Hyperquenched Ti-Ni Hydrided by Electrolytic Hydrogen at 25-Degrees-C and Thermally Activated Hydrogen Gas-Relation between Tinihx Structure and Its Hydrogen Storage Capacity. *J. Appl. Electrochem.* **1997**, *27*, 598–604. [CrossRef]

22. Hagi, H.; Mizuno, M.; Ibe, T. Hydrogen pickup and formation of hydride in 50.9at%Ni-Ti alloy by cathodic polarization. *J. Surf. Finish. Soc. Jap.* **1997**, *48*, 337–342. [CrossRef]

23. Pelton, A.; Trépanier, C.; Gong, X.-Y.; Wick, A.; Chen, K.C. Structural and Diffusional Effects of Hydrogen in TiNi. In Proceedings of the International Conference on Shape Memory and Superelastic Technologies SMST 2003, Asilomar Conference Center, Pacific Grove, CA, USA, 5–8 May 2003; Duerig, T.W., Pelton, A., Eds.; SMST Society Inc.: Monterey, CA, USA, 2003; pp. 33–42.

24. Ilyin, A.A.; Nazimov, J.P.; Nikitich, A.S.; Chertov, S.I.; Gozenko, N.N.; Skvortsova, S.V. The effect of hydrogenation on the structure and properties of TH1 alloy. *Technol. Light Alloys* **1984**, *3*, 42–47. (In Russian)

25. Shorshorov, M.; Stepanov, I.; Flomenblit, Y.; Travkin, V. Phase and structure transformation induced by hydrogen in alloys on a titanium nickelide base. *Phys. Met. Metallorg.* **1985**, *60*, 109–123.

26. Shorshorov, M.K.; Flomenblit, Y.M.; Maslenkov, S.B.; Budigina, N.B. Causes of the inducing effect of hydrogen on thermoelastic martensitic transformations in alloys based on nickel–titanium intermetallics. *Fiz. Met. Metalloved.* **1987**, *64*, 498–503. (In Russian)

27. Maslenkov, S.B.; Budigina, N.B.; Shorshrov, M.K.; Flomenblit, Y.M. Shape memory effects, phase and structural transformations causes by hydrogen in alloys of the Ti-Ni system. *Phys. Met. Metallogr.* **1988**, *66*, 90–96.

28. Tomita, M.; Yokoyama, K.; Asaoka, K.; Sakai, J. Hydrogen thermal desorption behavior of Ni–Ti superelastic alloy subjected to tensile deformation after hydrogen charging. *Mater. Sci. Eng. A* **2008**, *476*, 308–315. [CrossRef]

29. Horikawa, K.; Kawabata, Y.; Kobayashi, H. Spontaneous Bending of Ni–Ti Alloys Plates Caused by Preferential Hydrogen Absorption. *Mater. Trans.* **2008**, *49*, 2233–2237. [CrossRef]

30. Yokoyama, K.; Hashimoto, T.; Sakai, J. First interactions between hydrogen and stress-induced reverse transformation of Ni–Ti superelastic alloy. *Phil. Mag. Lett.* **2017**, *97*, 459–468. [CrossRef]

31. Yokoyama, K.; Eguchi, T.; Asaoka, K.; Nagumo, M. Effect of constituent phase of Ni–Ti shape memory alloy on susceptibility to hydrogen embrittlement. *Mater. Sci. Eng. A* **2004**, *374*, 177–183. [CrossRef]

32. Mirkin, L.I. *X-Ray Control of Engineering Materials*; Mashinostroenie: Moscow, Russia, 1979; p. 134. (In Russian)

33. Reidinger, F.; Lynch, J.F.; Reilly, J.J. An x-ray diffraction examination of TiFe–H_2 system. *J. Phys. F Met. Phys.* **1982**, *12*, 49–55. [CrossRef]

34. Otsuka, K.; Ren, X. Physical metallurgy of Ti–Ni-based shape memory alloys. *Prog. Mater. Sci.* **2005**, *50*, 511–678. [CrossRef]